ELSEVIER

International Journal of Minerals, Metallurgy and Materials
Volume 16, Number 4, August 2009, Page 414

Materials

Corrosion behavior and mechanism of the automotive hot-dip galvanized steel with alkaline mud adhesion

Hong Zhang[1)], *Xiao-gang Li*[1)], *Cui-wei Du*[1)], *and Hui-bin Qi*[2)]

1) School of Materials Science and Engineering, University of Science and Technology Beijing, Beijing 100083, China
2) Institute of Welding and Surface Technology, Baoshan Iron & Steel Co. Ltd., Shanghai 201900, China
(Received 2008-07-19)

Abstract: The corrosion behavior and mechanism of hot-dip galvanized steel and interstitial-free (IF) substrate with alkaline mud adhesion were investigated by scanning electron microscopy (SEM), X-ray diffraction (XRD), electrochemical impedance spectroscopy (EIS), and linear polarization. The results show that non-uniform corrosion occurs on the galvanized steel and IF substrate during 250 h with the mud adhesion. The corrosion products on the galvanized steel are very loose and porous, which are mainly ZnO, $Zn_5(OH)_8C_{l2}\cdot H_2O$ and $Zn(OH)_2$, and Fe-Zn alloy layer with a lower corrosion rate is exposed on the galvanized steel surface; however, the corrosion products on IF substrate are considerably harder and denser, whose compositions of rust are mainly FeOOH and Fe_3O_4, and several pits appear on their surface. The results of continuous EIS and linear polarization measurements exhibit a corrosion mechanism, that is, under activation control, the charge transfer resistances present different tendencies between the galvanized steel and IF substrate; in addition, the evolution of linear polarization resistances is similar to that of charge transfer resistances. The higher contents of dissolved oxygen and Cl^- ions in the mud play an important role in accelerating the corrosion.

Key words: corrosion mechanism; galvanized steel; interstitial-free (IF) steel; mud; adhesion

[*This work was financially supported by the National Natural Science Foundation of China (No.50571022), and the National Science & Technology Infrastructure Development Program of China (No.2005DKA10400).*]

1. Introduction

The hot-dip galvanized coating displays superior inherent corrosion protection. Numerous researches have been carried out on the corrosion behavior and mechanism of the galvanized steel in atmosphere and NaCl solution [1-4]. Furthermore, Romanoff *et al.* [5] tried to perform some experiments in soil. However, there are few discussions on the corrosion behavior of the galvanized steel with the mud adhesion. When an automobile runs on the road, the splash and deposition of the snowmelt salt and mud frequently occur on the surface of the automotive sheet. If not cleaned in time, some corrosion types, such as general corrosion, crevice corrosion, pitting corrosion, and galvanic corrosion, and so on, often occur. Generally, these details are difficult to discover and can result in serious corrosion on the automotive sheet. This is because the corrosion with the mud adhesion is very complicated and is different from ordinary electrolyte characteristics. Based on the analysis, this article presented the proposed research carried out on the local corrosion behavior and mechanism of the automotive galvanized steel sheet made in China, mainly using adhesion corrosion tests of the mud which was made in typical Ku'erle desert and saline soil. In addition, electrochemical impedance spectroscopy (EIS) and linear polarization were used for *in-situ* determining the corrosion rate of the galvanized steel sheet and interstitial-free (IF) substrate.

2. Experimental

2.1. Preparation of the sample and medium

Specimens were prepared from an automotive hot-dip galvanized steel sheet of 0.7 mm in thickness with a 75 $g\cdot m^{-2}$ zinc (0.15wt% Al) coating made in China by cutting specimens into a small plate with the dimension 30 mm×30 mm. The galvanized plates were not chemically treated. A small pore was made

Corresponding author: Hong Zhang, **E-mail:** hongzhang0523@163.com

Also available online at www.sciencedirect.com

in a corner of the sample, and an insulated wire with the skinning of 10 mm in length crossed the hole with an exact fit to the sample, which was sealed with a fluid sealant. Finally, the conducting state between them was ensured. The primitive surfaces of the samples were adopted after cleaning.

The underlying substrate of the galvanized steel was IF steel, and its composition is shown in Table 1.

Table 1. Chemical composition of the substrate of galvanized steel sheets **wt%**

C	Si	Mn	P	S	Cu	Ni	Cr	Sn	Nb	V	Al	Ti	Fe
0.0028	0.0100	0.1400	0.012	0.0062	0.0200	0.0100	0.0100	0.0020	0.0010	0.0010	0.0390	0.0410	Bal.

The hot-dip galvanized steel sheet with an average coating thickness of 16 μm was used as the experimental material. Fig. 1 shows the scanning electron microscopy (SEM) photograph and energy dispersive spectrometer (EDS) results of the cross section of the samples. It could be seen that the coating layers were composed of two phases, η phase (Zn) and ξ phase ($FeZn_{13}$), and the alloy layers were found to contain a small amount of Al.

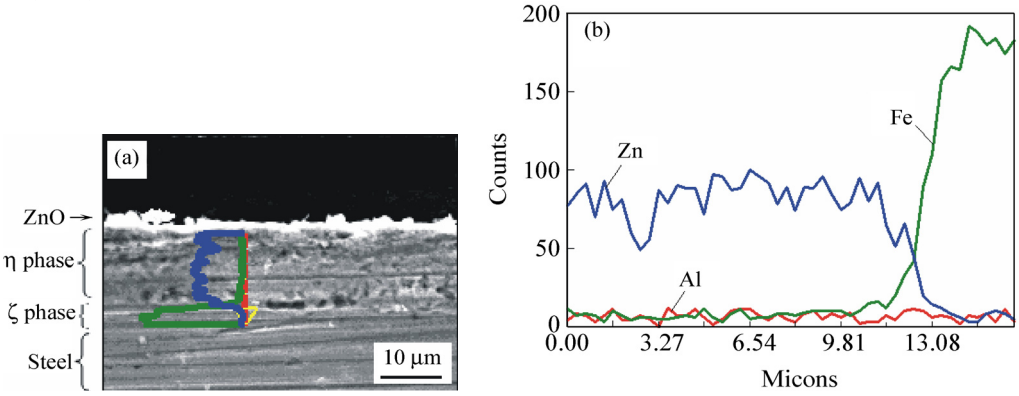

Fig. 1. SEM photograph and EDS results of the cross section of the sample.

The test mud was made of Ku'erle soil with high content of sand, its main physical and chemical data are shown in Table 2. This kind of soil was dried naturally, filtered with a 20 mesh sieve, and then dried at 105°C in an oven (6 h); after cooling, the soil with adding the de-ionized water was stirred to mix well to make the Ku'erle mud with 15wt% content water. This mud had good viscosity and no water exudation.

Table 2. Main physical and chemical data of the Ku'erle soil

Chemical composition / wt%							Electrical conductivity / ($mS \cdot cm^{-1}$)	pH
Cl^-	NO_3^-	SO_4^{2-}	Ca^{2+}	Mg^{2+}	K^+	Na^+		
0.1521	0.0091	0.2446	0.0910	0.0022	0.0041	0.1100	2.000	9.10

2.2. Test methods

The mud adhesion method was operated as the following: the galvanized steel specimen was kept horizontally and positioned in a container as illustrated in Fig. 2. The mud of 10 mm in thickness was covered on the surface of the steel and dried at 30°C with a relative humidity (RH) of 50%. The period of each experimental test was set to be 250 h and the sampling time was 24, 60, 100, 150, 200, and 250 h, respectively. The weights of the specimen and mud were regularly measured to ensure that they remained constant. Otherwise, de-ionized water was added to balance the evaporation of water from the mud. The samples with the mud adhesion up to 250 h were taken for SEM observation and X-ray diffraction (XRD) analysis of corrosion products.

The samples after corrosion for various sampling time intervals were taken for EIS and linear polarization measurements. All measurements were performed at a stable open-circuit potential (OCP) of the system using EG&G PARSTAT 2273 electrochemical system. EIS measurements were conducted at OCP with a 10 mV/(rms) signal amplitude and the number of points was 40. The frequency range covered was from 100 kHz to 10 mHz. The experimental results were interpreted on the basis of an equivalent circuit determined using a suitable fitting procedure described in ZWin-Simp program (impedance data analysis system). The measurement extent of linear polarization was −10 mV to +10 mV at OCP.

3. Results

3.1. Macro-morphology features

The corrosion processes of the automotive galvanized steel and substrate changed differently under the adhesion of the Ku'erle mud. The macro-photographs

in different sampling time intervals are shown in Fig. 3 after cleaning the mud.

It can be seen from Fig. 3 that the surfaces of the galvanized steel sheet were tarnished and showed different patterns, and the corrosion was non-uniform for 24 h; with the adhesion time increasing, white products were produced, the color of the surface became murky gray, and the color differences reduced, and then, several gray-blue surfaces came out for 250 h.

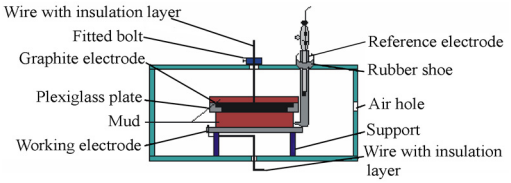

Fig. 2. Schematic of the electrochemical test under the mud adhesion.

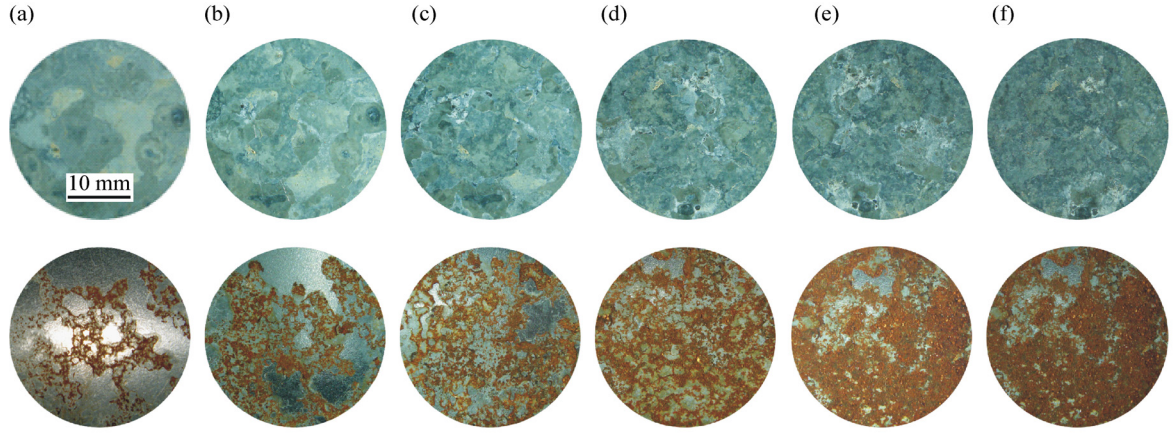

Fig. 3. Macro-photographs of the galvanized steel sheet (in upper row) and substrate (in nether row) for different time intervals of mud adhesion: (a) 24 h; (b) 60 h; (c) 100 h; (d) 150 h; (e) 200 h; (f) 250 h.

Equally, non-uniform corrosion occurred on the surface of the IF substrate. In the beginning of mud adhesion, very small amount of green rust was produced, which turned into yellow rust immediately; and then some red rust covered the surface. With time, more and more of the black rust was produced below the red rust.

3.2. SEM observation

Fig. 4 shows the SEM results of the several corroded samples with Ku'erle mud adhesion for 250 h. It was obvious that the products on the galvanized steel sheet were very porous (Fig. 4(a)), on which there were several needle-like products and they grew forming islands as the adhesion time increased. These crystals were believed to be $Zn_5(OH)_8Cl_2{\cdot}H_2O$ [6]; the products on the substrate were firm and compact (Fig. 4(b)); the gray-blue Fe-Zn alloy layer was exposed when the pure zinc almost disappeared (Fig. 4(c)); and several corrosion pits were produced on the substrate surface (Fig. 4(d)).

3.3. EIS measurements

Fig. 5 shows the EIS diagrams of various samples of the galvanized steel sheet and IF substrate with mud adhesion at different time intervals, which includes Nyquist plots (a) and (c), and Bode plots (b) and (d). In Nyquist plots, x-axis is the real parts of impedance Z_{Re}, and y-axis is the imaginary part of impedance Z_{Im}. In Bode plots, x-axis is the frequency of sine waves, and y-axis is the phase angles of impedance (Z).

It was obvious that the EIS results showed different evolutions. With regard to the galvanized steel sheet, the diameters of capacitive arcs first increased, then decreased, and expanded at last, and those of the IF substrate increased gradually before 200 h, and then decreased at 250 h. Two peaks were revealed obviously at both high and low frequencies in Bode-Phase plots (Fig. 5(b)), that is, two time constants were involved in the whole corrosion process of the galvanized steel sheet, and the phase shift angles of the IF substrate were in the high frequency domain and low frequency domain, respectively, and overlapped as a broadened peak [6]. It was possible that the EIS diagrams of galvanized steel sheet and IF substrate were all composed of two close time constants and overlapped some large capacitive arcs, and the diameters of capacitive arcs of the galvanized steel sheet were larger than those of the IF substrate in the same time.

No oxygen diffusion control character appeared during the whole process with the adhesion of the Ku'erle mud up to 250 h, and the charge transfer process was the control step. The construction of rust layer could be described based on the present observations using the equivalent circuit in Fig. 6. R_s represents the electrolyte resistance, C_r represents the rust capacitance, R_r represents the rust resistance, C_{dl} represents the double-layer capacitance, and R_{ct} represents the charge-transfer resistance.

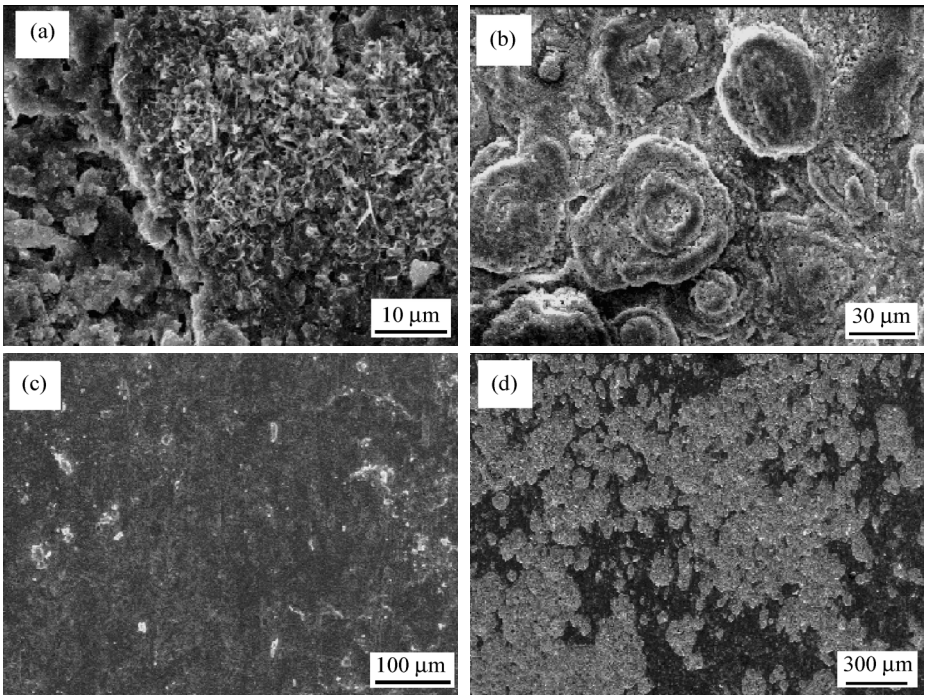

Fig. 4. SEM photomicrographs of the galvanized steel and substrate after Ku'erle mud adhesion up to 250 h: (a) corrosion products on the surface of the galvanized steel; (b) corrosion products on the surface of the IF substrate; (c) the surface of the galvanized steel after cleaning the products; (d) the surface of the IF substrate after cleaning the products.

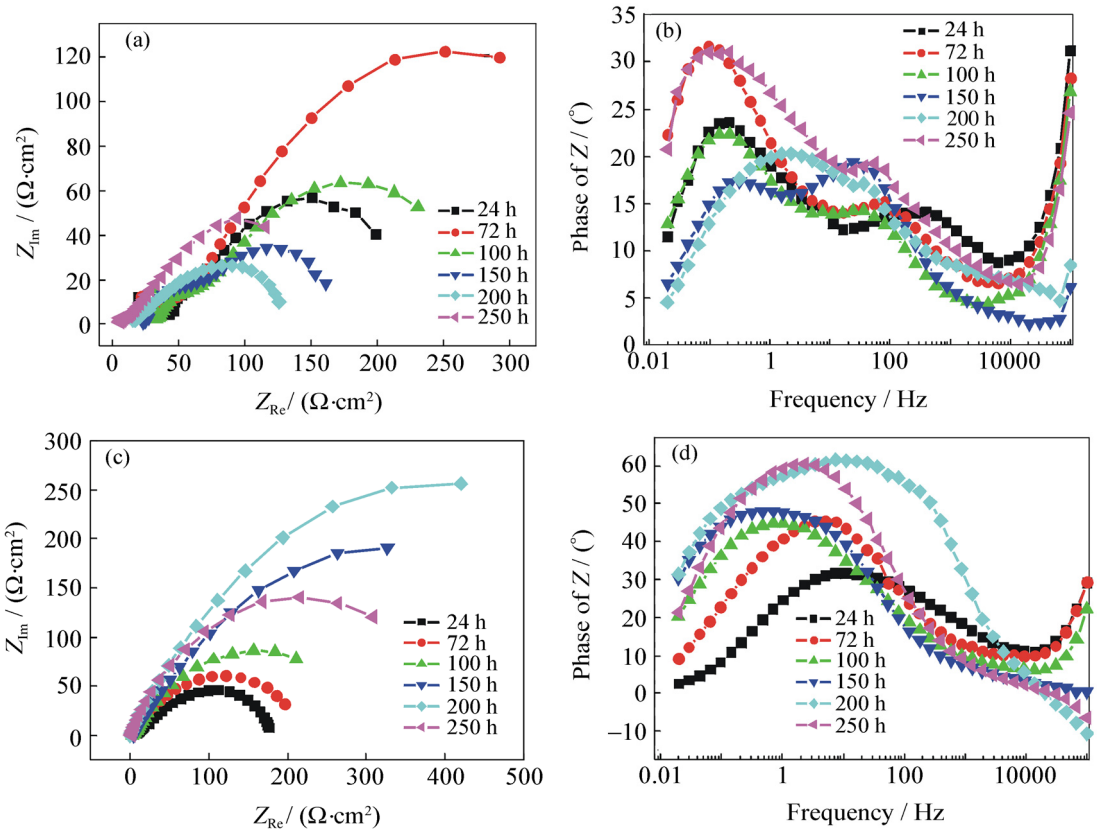

Fig. 5. EIS plots of the galvanized steel sheet and IF substrate under the adhesion of the Ku'erle mud: (a) Nyquist plots of the galvanized steel sheet; (b) Bode-phase plots of the galvanized steel sheet; (c) Nyquist plots of the IF substrate; (d) Bode-phase plots of the IF substrate.

Figs. 7(a)-(b) showed the R_{ct} and R_r of the described equivalent circuit. It was observed that R_{ct} of the galvanized steel sheet first increased, then decreased, and increased again, and that of the IF substrate increased before 200 h, and then decreased. On the other hand, the evolution of R_r of the galvanized steel sheet was similar to that of IF substrate, that is, it increased before 150 h, and then decreased.

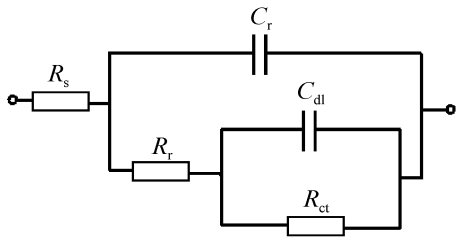

Fig. 6. Equivalent circuit used for fitting the impedance results of Fig. 5.

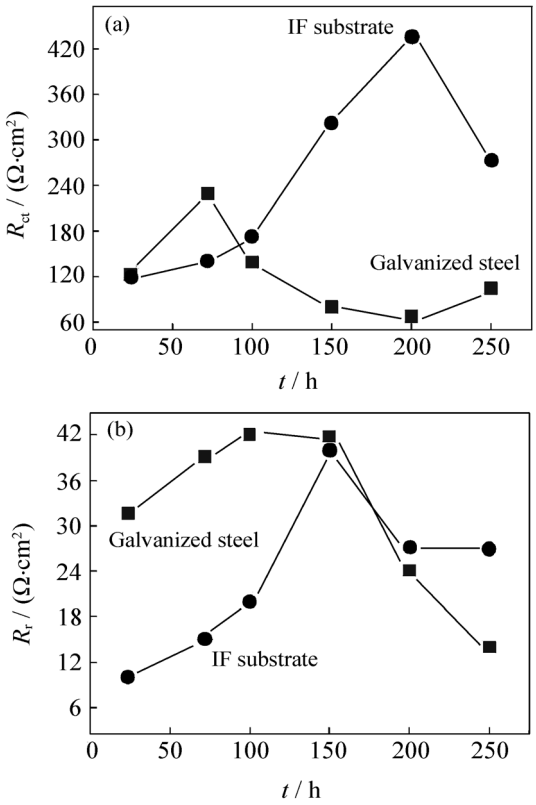

Fig. 7. Changes in charge transfer resistance and the resistance of barrier layer in pitting area of the galvanized steel and IF substrate with mud adhesion time: (a) charge transfer resistance (R_{ct}); (b) resistance of barrier layer (R_r) in pitting area.

3.4. Linear polarization measurement

Linear polarization measurements were carried out using the samples with different adhesion time intervals, and the results are shown in Fig. 8. It can be seen that the evolution of polarization resistance (R_p) was similar to that of charge transfer resistance (R_{ct}) of the galvanized steel sheet and IF substrate in Fig. 7, however, the polarization resistances were larger than the charge transfer resistances in the same time.

3.5. XRD analysis of corrosion products

The rust phases on the galvanized steel sheet and IF substrate were examined by *in-situ* XRD. Fig. 9 corresponds to samples after 250 h adhesion time. The results indicated that the main corrosion products of rust on the galvanized steel surface were ZnO, $Zn_5(OH)_8Cl_2{\cdot}H_2O$, and $Zn(OH)_2$ as shown in Fig. 9(a), and those on the IF substrate surface were FeOOH (outer layer) and Fe_3O_4 (inner layer) as shown in Fig. 9(b). Also, EDS analysis presented in Fig. 10 showed that the ingredients of the grey-blue area were mainly composed of Fe-Zn alloy phase.

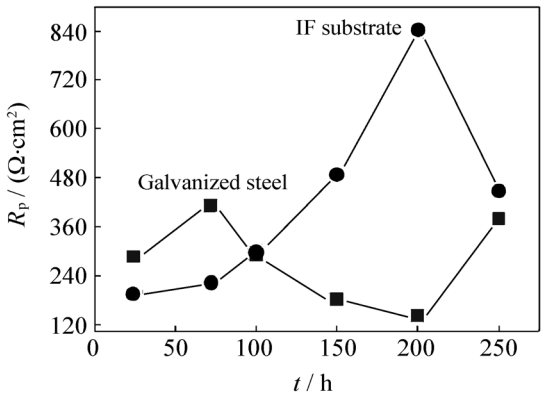

Fig. 8. Changes in the polarization resistance of the galvanized steel sheet and IF substrate.

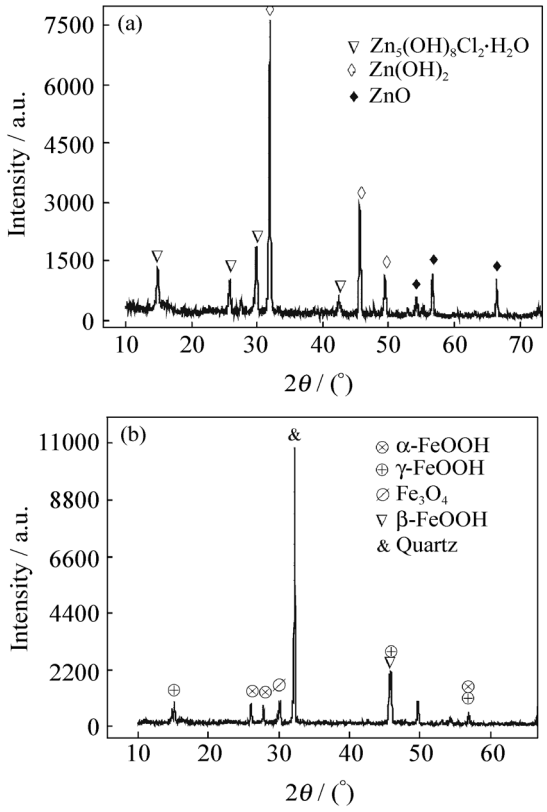

Fig. 9. *In-situ* XRD results after 250 h with mud adhesion: (a) galvanized steel; (b) IF substrate.

4. Discussion

4.1. EIS analysis

With increasing mud adhesion time, the EIS of the galvanized steel sheet and IF substrate exhibited two partially overlapped depressed arcs. At high frequencies, the time constant was associated with the integrity, density, and thickness of the barrier layer. At low

frequencies, the time constant was related to the charge transfer behavior of the electrode interface. On the other hand, EIS possessed no diffusion control feature; this was because the content of the sand in Ku'erle soil was numerous and irregularly sized, therefore, it was easy for the oxygen to diffuse to the surface of the samples.

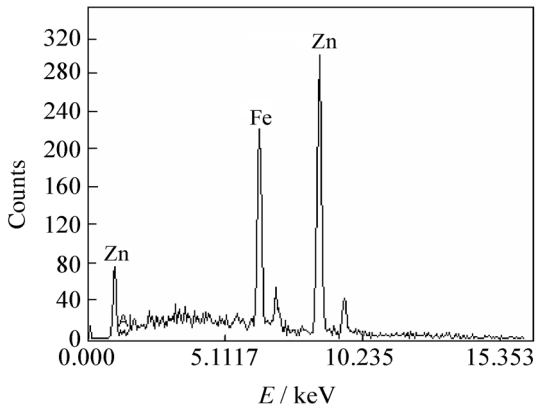

Fig. 10. EDS analysis results of the grey-blue area under the pure zinc layer of the galvanized steel.

At the beginning of the corrosion process with the mud adhesion, the associated chemical reactions of corrosion would affect preferentially the lower potential position on the surface of the electrode interface, such as the surrounding of inclusions and the inside of pits. The uneven liquid thin film was formed easily because of the higher content of the sand, and the area with the thicker liquid film produced severe corrosion to result in pitting.

Generally, accumulation formation of corrosion products can hinder further the reaction of the electrode [7]. The fresh surface of the galvanized steel sheet has a quick corrosion rate because of the enough dissolved oxygen with mud adhesion, therefore, the R_{ct} is smaller. With time, corrosion products together with mud on the surface of the galvanized steel sheet form a barrier layer to decrease the corrosion rate, and cause R_{ct} to increase. Otherwise, the corrosion products are very porous and combined easily with mud, thus, they form some crevices together with the penetration of Cl^- ions to result in local corrosion. This makes the zinc coating to further dissolve when R_{ct} reduces. After a long period, the amount of the corrosion products increase gradually, and the thickness of the barrier layer also increases in the meantime. In addition, when the zinc coatings almost corrode completely, Fe-Zn alloy layer comes up to be a protective layer to prevent the steel from further corrosion [8] leading to a higher R_{ct}.

Likewise, a non-uniform liquid film layer forms on the surface of the IF substrate with the mud adhesion to cause local corrosion. At the beginning of the corrosion process, the corrosion rate is lower owing to the smaller surface roughness and denser organizational structure, therefore, R_{ct} leads to a smaller increase. With the increase of mud adhesion time, the corrosion rate increases gradually, and the amount of corrosion products increases again in the same time. These products combine with mud and form a dense barrier layer to bring about R_{ct} increase quickly. The rust layer is composed of inner layer and outer layer, and the latter is very fragile to separate from the former easily. Some crevices form to accelerate the corrosion, thus, the R_{ct} value decreases.

Corrosion products forming combined with mud on the surface of the galvanized steel sheet produce a special barrier layer, which results in rust and the resistance R_r on the pitting area reaching a maximum at 100 h. To a certain extent, this barrier layer separates from the galvanized steel to form some crevices and decreases the resistance of the barrier, and thus, the R_r value goes down gradually. The R_r evolution of the IF substrate is similar to that of the galvanized steel sheet.

Moreover, a larger amount of corrosion products combined well with mud fill some gap in mud and formed a denser barrier layer. Comparatively speaking, the corrosion products of the IF substrate are harder and difficult to fill some gap, therefore, the R_r values are smaller than those of the galvanized steel in the same time. Using these two parameters, R_{ct} and R_r, it is useful to explain the corrosion behavior electrochemically.

4.2. Linear polarization analysis

According to the results of Fig. 7(a) and Fig. 8, the evolution of R_p was similar to that of R_{ct} and exhibited a good correlation. Moreover, the R_p values were all larger than the R_{ct} values in the same time, respectively.

As well known, by definition of the polarization resistance (R_p), $R_p=(Z_F)_{\omega=0}$, where Z_F is the faradaic impedance. At the site where the left end of the capacitive arc intersects with the real axis, that is to say, as $\omega\to\infty$, $Z_{Re}=R_s$; and at the site where the right end of the capacitive arc intersects with the real axis, EIS is decided by circuit $R_s(C_r(R_r(C_{dl}R_{ct})))$. As $\omega=0$,

$$Z_{Re}=R_s + R_p=R_s + R_{ct} + R_r$$

where ω is the angular frequency. Therefore, $R_p>R_{ct}$.

The R_p values obtained from linear polarization were the overall performance of the equivalent circuit. The increase of polarization resistance R_p or charge

transfer resistance R_{ct} indicated the lower rate of reduction. Thus, the R_p values were very useful in comparing qualitatively the rate of the corrosion process.

4.3. Corrosion mechanisms analysis

During adhesion corrosion of the Ku'erle mud, larger content of the sand in this mud resulted in forming a non-uniform electrolyte liquid film. This caused oxygen-concentration cell corrosion easily. The local corrosion occurred on the surfaces of the galvanized steel sheet and IF substrate. Especially, Cl^- ions in the mud not only accelerated the corrosion, but also took part in the reaction.

The corrosion products and conductibility were influenced by the contents of the salt, components, and acidity and alkalinity in mud [4]. Ku'erle mud was alkaline and had a larger content of Cl^- ions. These factors affected the corrosion rate and mechanisms.

Zinc oxide (ZnO) formed easily on the zinc surface with the adhesion of alkaline mud, which further formed other corrosion products. Penetration of Cl^- ions resulted in the corrosion rate increasing continually. Since mud had a lower fluidity, the corrosion products were difficult to be transferred in time. With the evolution of corrosion, the deposition weight of the corrosion products on the surface of the zinc coating increased gradually. In the meantime, insoluble zinc hydroxychloride ($Zn_5Cl_2(OH)_8 \cdot H_2O$) was produced, which reduced the corrosion rate.

Cl^- ions were one of the important factors of zinc and a zinc coating in some environments [9] and strong anodic activator. As Cl^- ions adsorbed on some passive films, they destroyed high alkaline environment on the surface of the samples by means of local acidulation and reduced the pH value of the surface of the samples to dissolve the passive films. Then, the local corrosion was produced on the surface of the galvanized steel sheet and IF substrate under enough O_2 and H_2O. The electrochemical corrosion mechanism was: after Cl^- ions destroyed some of the passive films, the metal substrate appeared and acted as an anode, and others of the intact massive passive films acted as a cathode, therefore, they formed some activation-inactivation corrosion cells. Owing to the smaller anode *vs.* the larger cathode, this resulted in accelerating the pitting corrosion.

With the electric current flowing, Cl^- ions in the Ku'erle mud transferred to the pits and maintained the state of activation of the zinc surface in pits. On the other hand, the hydrolysis reaction of Cl^- ions and acidity in the pits increased and promoted the pitting corrosion, and formed an autocatalysis process.

Based on the above analysis, the corrosion reactions of the galvanized steel sheets and IF substrates are expressed as the following equations with the adhesion of the Ku'erle mud.

The anodic reactions [10-11]:

$$Zn \rightarrow Zn^{2+} + 2e \quad (1)$$

$$Zn + 2OH^- \rightarrow ZnO + H_2O + 2e \quad (2)$$

$$Zn + 4H_2O \rightarrow Zn(OH)_2 + 2H_3O^+ + 2e \quad (3)$$

$$ZnO + Zn^{2+} + 2Cl^- + 5H_2O \rightarrow Zn_5Cl_2(OH)_8 \cdot H_2O \quad (4)$$

The IF substrate first caused anodic dissolution with the mud adhesion and produced Fe^{2+}, then turned into green rusts [12], and later developed into plenty of non-crystalline solids and a small amount of β-FeOOH and α-FeOOH. γ-FeOOH in rusts was transformed from β-FeOOH. The non-crystalline iron Fe^{2+} and Fe^{3+} oxide crystallized and turned into Fe_3O_4. In addition, β-FeOOH and γ-FeOOH produced Fe_3O_4 by reduction reactions [13]. The anodic dissolution of iron was suppressed gradually by accumulating Fe_3O_4 and α-FeOOH, which had a lower chemical activity.

The corrosion reactions of the IF substrate are expressed as the following equations with the adhesion of the Ku'erle mud.

The anodic reactions [14-16]:

$$Fe \rightarrow Fe^{2+} + 2e \quad (5)$$

$$Fe^{2+} + 2Cl^- + 4H_2O \rightarrow FeCl_2 \cdot 4H_2O \quad (6)$$

$$FeCl_2 \cdot 4H_2O \rightarrow Fe(OH)_2 + 2Cl^- + 2H^+ + 2H_2O \quad (7)$$

$$Fe^{2+} + 2OH^- \rightarrow Fe(OH)_2 \quad (8)$$

$$4Fe(OH)_2 + O_2 + 2H_2O \rightarrow 4Fe(OH)_3 \quad (9)$$

$$2[Fe \cdot OH]^+ + O_2 + 2e \rightarrow 2FeOOH \quad (10)$$

$$2[Fe \cdot OH]^+ \cdot nH_2O + O_2 + 2e \rightarrow 2FeOOH \cdot nH_2O \quad (11)$$

$$2Fe(OH)_3 \rightarrow Fe_2O_3 + 3H_2O \quad (12)$$

$$2Fe(OH)_3 + Fe(OH)_2 \rightarrow Fe_3O_4 + 4H_2O \quad (13)$$

$$\gamma\text{-FeOOH} \rightarrow \alpha\text{-FeOOH} \quad (14)$$

$$3FeOOH + e \rightarrow Fe_3O_4 + H_2O + OH^- \quad (15)$$

The oxygen reduction was the cathodic reaction:

$$O_2 + 2H_2O + 4e \rightarrow 4OH^- \quad (16)$$

According to the above analysis, it was obvious that the experimental results were in good agreement. On the other hand, the corrosion rate of the galvanized steel sheet was different from that of the IF substrate, and their corrosion mechanisms were very complicated. Therefore, it was very necessary to further study the questions of the mud adhesion in more detail

and depth.

5. Conclusions

(1) During the alkaline mud adhesion for 250 h, non-uniform corrosion is caused on the galvanized steel sheet and IF substrate. The corrosion products on the galvanized steel sheet are very loose and porous, and that of the IF substrate is harder and denser. Fe-Zn alloy layer is observed on some areas of the galvanized steel, which has a lower corrosion rate as compared to a pure zinc coating, and several pits are observed on the surface of the IF substrate.

(2) The results obtained by continuous EIS measurements for 250 h exhibit a corrosion mechanism, that is, under activation control. The evolution of charge transfer resistance of the galvanized steel increases firstly, then decreases, and increases again; however, that of the IF substrate increases gradually to a maximum, and then decreases. On the other hand, the evolution of polarization resistances obtained by linear polarization measurements is similar to the results of charge transfer resistance by EIS measurements.

(3) With mud adhesion up to 250 h, the corrosion products of the galvanized steel are mainly ZnO, $Zn_5(OH)_8C_{l2}{\cdot}H_2O$, and $Zn(OH)_2$, and those of the IF substrate are FeOOH (outer layer) and Fe_3O_4 (inner layer).

(4) Enough dissolved oxygen and higher Cl^- contents have to be taken into account while explaining the corrosion behavior for 250 h of the galvanized steel and IF substrate.

References

[1] M.A. Arenas and J. Damborenea, Use of electrochemical impedance spectroscopy to study corrosion of galvanized steel in 0.6M NaCl solution, *Corros. Eng. Sci. and Technol.*, 41(2006), No.3, p.228.

[2] D.A. Worsley, H.N. Mcmurray, J.H. Sullivan, and I.P. Williams, Quantitative assessment of localized corrosion occurring on galvanized steel samples using the scanning vibrating electrode technique, *Corrosion.*, 60(2004), No.5, p.437.

[3] V. Barranco, S. Feliu, and J.S. Feliu, EIS study of the corrosion behavior of zinc-based coatings on steel in quiescent 3% NaCl solution. Part 1: Directly exposed coatings, *Corros. Sci.*, 46(2004), No.9, p.2203.

[4] Z.Y. Wang, G.C. Yu, and W. Han, Atmospheric corrosion law of three non-ferrous metals in Shenyang area, *Trans. Nonferrous Met. Soc. Chin.* (in Chinese), 13(2003), No.2, p.367.

[5] X.G. Zhang, Corrosion of the zinc and zinc alloy, *Corros. Prot.* (in Chinese), 27(2006), No.2, p.99.

[6] P.R. Sere, M. Zapponi, C.I. Elsner, and A.R. Di Sarli, Comparative corrosion behavior or 55Aluminum-Zinc alloy and zinc hot-dip coatings deposited on low carbon steel substrates, *Corros. Sci.*, 40(1998), No.10, p.1711.

[7] Q.X. Sun, J.Q. Zhang, and C.J. Lin, Quantitatively predicate state of adhesion between coating/metal interface by EIS measurements, *Acta Phys. Chim. Sin.* (in Chinese), 20(2004), No.11, p.1299.

[8] A.P. Yadav, H. Katayama, K. Noda, *et al.*, Effect of Fe-Zn alloy layer on the corrosion resistance of galvanized steel in chloride containing environments, *Corros. Sci.*, 49(2007), No.9, p.3716.

[9] J.T. Nurmi and P.G. Tratnyek, Electrochemical studies of packed iron powder electrodes: effects of common constituents of natural waters on corrosion potential, *Corros. Sci.*, 50(2008), No.1, p.148.

[10] S.C. Chung, A.S. Lin, J.R. Chang, and H.C. Shih, EXAFS study of atmospheric corrosion products on zinc at the initial stage, *Corros. Sci.*, 42(2000), No.9, p.1599.

[11] F. Zhu, D. Persson, D. Thierry, and C. Taxen, Formation of corrosion products on open and confined zinc surfaces exposed to periodic wet/dry conditions, *Corrosion.*, 56(2000), No.12, p.1256.

[12] I. Suzuki, N. Masuko, and Y. Hisamatsu, Electrochemical properties of iron rust, *Corros. Sci.*, 19(1979), No.8, p.530.

[13] T. Nishimura, H. Katayama, K. Noda, and T. Kodama, Electrochemical behavior of rust formed on carbon steel in a wet/dry environment containing chloride ions, *Corros.*, 56(2000), No.9, p.935.

[14] M.H. Jin, S.L. Meng, H.T. Huang, and G.H. Du, Corrosion mechanism of carbon steel in four types of soil, *J. Huazhong Univ. Sci. Technol.* (in Chinese), 30(2002), No.7, p.104.

[15] L. Legrand, G. Sagon, S. Lecomte, *et al.*, A Raman and infrared study of a new carbonate green rust obtained by electrochemical way, *Corros. Sci.*, 43(2001), No.9, p.1739.

[16] S.K. Kwon, K. Shinoda, S. Suzuki, and Y. Waseda, Influence of silicon on local structure and morphology of γ-FeOOH and α-FeOOH particles, *Corros. Sci.*, 49(2007), No.3, p.1513.